JOURNAL OF SYNCHROTRON RADIATION
ISSN 1600-5775

A compact furnace for *in situ* X-ray absorption spectroscopy: design, fabrication and study of cationic oxidation states in Pr_6O_{11} and NiO

Suchinda Sattayaporn,[a]* Somboonsup Rodporn,[a] Pinit Kidkhunthod,[a] Narong Chanlek,[a] Chutarat Yonchai[a] and Saroj Rujirawat[b,c]

[a]Synchrotron Light Research Institute, Nakhon Ratchasima 30000, Thailand, [b]School of Physics, Institute of Science, Suranaree University of Technology, Nakhon Ratchasima 30000, Thailand, and [c]Research Network NANOTEC-SUT on Advanced Nanomaterials and Characterization, School of Physics, Institute of Science, Suranaree University of Technology, Nakhon Ratchasima 30000, Thailand. *Correspondence e-mail: suchinda@slri.or.th

Received 8 October 2020
Accepted 30 November 2020

Edited by K. Kvashnina, ESRF – The European Synchrotron, France

Keywords: X-ray absorption spectroscopy; *in situ* cells; transmittance and fluorescence; instrumentations; *in situ* XAFS.

A well designed compact furnace has been designed for *in situ* X-ray absorption spectroscopy (XAS). It enables various heat ramps from 300 K to 1473 K. The furnace consists of heaters, a quartz tube, a circulated refrigerator and a power controller. It can generate ohmic heating via an induction process with tantalum filaments. The maximum heating rate exceeds 20 K min^{-1}. A quartz tube with gas feedthroughs allows the mixing of gases and adjustment of the flow rate. The use of this compact furnace allows *in situ* XAS investigations to be carried out in transmission or fluorescence modes under controlled temperature and atmosphere. Moreover, the furnace is compact, light and well compatible to XAS. The furnace was used to study cationic oxidation states in Pr_6O_{11} and NiO compounds under elevated temperature and reduced atmosphere using the *in situ* X-ray absorption near-edge structure (XANES) technique at beamline 5.2 SUT-NANOTEC-SLRI of the Synchrotron Light Research Institute, Thailand. At room temperature, Pr_6O_{11} contains a mixture of Pr^{3+} and Pr^{4+} cations, resulting in an average oxidation state of +3.67. *In situ* XANES spectra of Pr (L_3-edge) show that the oxidation state of Pr^{4+} cations was totally reduced to +3.00 at 1273 K under H_2 atmosphere. Considering NiO, Ni^{2+} species were present under ambient conditions. At 573 K, the reduction process of Ni^{2+} occurred. The Ni^0/Ni^{2+} ratio increased linearly with respect to the heating temperature. Finally, the reduction process of Ni^{2+} was completely finished at 770 K.

1. Introduction

X-ray absorption spectroscopy (XAS) performed at synchrotron sources has been considered a powerful characterization tool for several decades due to its high sensitivity and its capability to probe almost all elements of the periodic table. This technique is non-destructive and is suitable for studying a large variety of materials such as powders, solids, liquids, glasses, thin films, crystals and amorphous compounds. Basically, XAS spectra consist of X-ray absorption near-edge structure (XANES) and extended X-ray absorption fine structure (EXAFS). The XAS spectra can be used to determine the cationic/anionic oxidation state, chemical geometry, coordination number, oxygen vacancy and local structure of a probed element. Therefore, it is frequently used to sustainably develop physical, thermo-electric, catalytic or magnetic properties of advanced and novel materials (Yao *et al.*, 2019; Song *et al.*, 2019; Jaiban *et al.*, 2018; Sumrunronnasak *et al.*, 2018; Sriplai *et al.*, 2018; Boonruang *et al.*, 2018). It is well known that the performance of the XAS technique can be

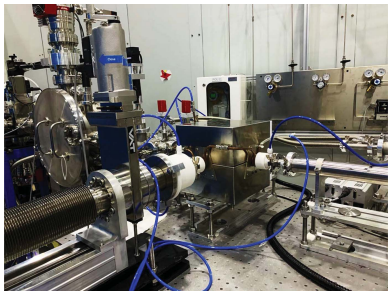

enhanced by utilizing *in situ* cells which enable experimental conditions, such as elevated temperature, vacuum, inert and reducing/oxidizing atmosphere, to be controlled in real time. According to the literature, *in situ* heating cells have been developed using different approaches for time- or temperature-resolved XAS techniques (Tamura *et al.*, 1995; Lamberti *et al.*, 2003; Huwe & Fröba, 2004; Meneses *et al.*, 2006; An *et al.*, 2014; Yamamoto *et al.*, 2018; Zhao *et al.*, 2017; Inukai *et al.*, 2015). Most were initially fabricated for the purpose of XAS investigations on catalyst materials (van Bokhoven *et al.*, 1999; van der Eerden *et al.*, 2000; Grunwaldt *et al.*, 2001; Kappen *et al.*, 2001; Bolin *et al.*, 2013; Yamamoto *et al.*, 2018; Mathisen *et al.*, 2018). Recently, the *in situ* XAS technique has also been applied to characterize other advanced and novel materials (Steiner *et al.*, 2019; Deb *et al.*, 2006; Hashimoto *et al.*, 2007; Massa *et al.*, 2015; Marini *et al.*, 2018; Mastelaro *et al.*, 2018; Chin *et al.*, 2019). Nevertheless, these *in situ* heating cells possess some limitations in terms of maximum temperature, heating rate, flowing gas or measurement mode. Therefore, it has been interesting to design an *in situ* XAS furnace with optimized functionalities and qualities.

In this work, we demonstrate the design, thermal simulation, fabrication and performance tests for an *in situ* XAS furnace. The compact furnace was designed simply using inexpensive materials. The sample holder is designed to be adaptable for *in situ* transmission and fluorescence XAS measurements. The furnace can be easily installed at XAS synchrotron facilities and combined with gas lines. To the best of our knowledge, the compact *in situ* furnace possesses superior specifications to the previously mentioned *in situ* heating cells in terms of maximum temperature, heating rate and capability to perform XAS measurements in both transmission and fluorescence modes. In addition, the furnace atmosphere can be controlled by pumping under vacuum or flowing any type of gas such as H_2, N_2, O_2, Ar, He or CO_2 with an adjustable rate between 1 and 100 ml min^{-1}. Finally, we tested the quality and performance of the fabricated compact furnace at beamline 5.2 SUT-NANOTEC-SLRI XAS at the Synchrotron Light Research Institute (SLRI), Nakhon Ratchasima, Thailand, which is capable of tuning X-ray energy from 1.2 keV to 13.0 keV. *In situ* XAS experiments were operated from 300 K to 1473 K under H_2 atmosphere. The XANES experiments were performed by probing Pr and Ni elements at the L_3-edge and *K*-edge in transmission and fluorescence modes, respectively. The obtained spectra were normalized using *Athena* software (Ravel & Newville, 2005). A linear combination fit was also performed to investigate changes in the oxidation states and weight percentages of cationic ions in Pr_6O_{11} and NiO compounds.

Based on conventional XAS measurements in the tender X-ray range at beamline 5.2, SLRI, such a probing Si, Mg or Al XANES/EXAFS experiment could be performed by using double single-crystals of beryl ($10\bar{1}0$) as a monochromator and sealing the photon-in and photon-out windows with polypropylene tape. Note that a flowing He atmosphere is necessary to obtain a good XAS signal.

2. *In situ* compact furnace

The compact furnace was designed and developed to achieve high performances and optimal functionalities for *in situ* XAS measurement. The furnace system consists of four main components. First, a compact furnace equipped with a thermocouple and a proportional integral derivative (PID) controller. The PID controller has a set of digital temperature programs, including two patterns; the maximum number of steps is 16. Second, a three-way quartz tube, used as the sample holder. Third, flanged windows, enclosing the quartz tube for the photon-in pathway A and the photon-out pathways B and C. The windows are sealed by Kapton (polyimide) tape of thickness 50 µm. Kapton can be replaced by another window material such as polypropylene or beryllium, depending on the X-ray energy range. Furthermore, the feedthroughs of the gas inlet and outlet, mounted at the flange windows, allow the distribution of various types of gas such as H_2, N_2, He, Ar, CO_2 and O_2 into the quartz tube. The flow rate can be adjusted from 1 to 100 ml min^{-1} with gas mass flow controllers. Fourth, a cooling chamber, connected to a water-circulated refrigerator. It should be noted that flowing He gas is suggested during XAS measurements at photon energies below 3000 eV in fluorescence mode to improve the signal-to-noise ratio; above 3000 eV, experiments can be performed under air. Fig. 1 shows the construction drawing of the entire compact furnace; specifications of the compact furnace are summarized in Table 1. The main components of the *in situ* furnace are depicted and detailed in Fig. 2 and Table 2, respectively.

A thermal simulation was also conducted for the entire area of the furnace using *SolidWorks* (https://www.solidworks.com/) software as shown in Fig. 1 (inset). The heating zone was uniformly distributed and covered all of the furnace's body, precisely in an area of 100 mm × 100 mm. With these specifications, the maximum temperature can exceed 1473 K. The heating rate can be varied between 1 and 20 K min^{-1}. The furnace is equipped with a PID controller, enabling 16 heating steps to be programmed. Moreover, a sample holder was specially designed to be adaptable for measuring *in situ* XAS in transmission and fluorescence modes. Hence, the ceramic holder was cut and mounted at angles of 45° and 90°. Here, the sample holder can be put inside the three-ways quartz tube and placed together in the middle of the furnace.

Regarding Fig. 1, the monochromatic X-ray beam enters via entrance A and reaches the sample at the furnace center. In the case of transmission mode, the X-ray beam penetrates the sample and passes through the ionization chamber via pathway B. On the other hand, fluorescence emission can occur and is measured by using a solid-state detector at the end of pathway C. Here, we used a silicon drift detector (SDD), which is extremely sensitive to elevated temperature. Therefore, we fabricated a cooling chamber to prevent heat damage during *in situ* XAFS measurement. It was inserted between the heating zone and the SDD (see '5' in Fig. 1). This chamber has a window flange at the end, equipped with a high-

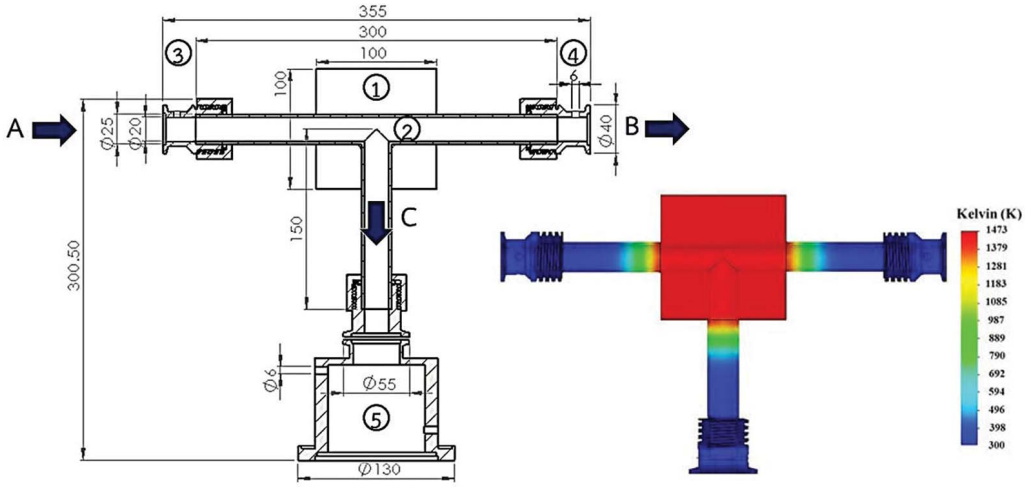

Figure 1
Construction drawing of the compact furnace with labeled lengths in millimetres and thermal simulation of the entire compact furnace in K (inset).

Table 1
In situ heating cell specifications and parameters.

Specifications	Details
Cell dimensions (length × width × height)	230 × 230 × 230 mm
Isolator type	Ceramic fiber broad (1873 K)
Stainless steel thickness	2.5 mm
Sample–transmission distance	30 mm
Sample–fluorescence distance	30 mm
Temperature range	273–1473 K
Heating rate range	1–20 K min^{-1}
Heater power	1.3 KW
Heater voltage	220 V
Thermocouple	Pt 10% Rh / Pt (R-type)
Constant-temperature area	100 × 100 mm
Total number of heating steps	16

Table 2
Main components of the *in situ* compact furnace.

Number	Item	Material
1	Furnace body (bottom)	Heater, ceramic (Al_2O_3), stainless steel
2	Furnace body (top)	Stainless steel
3	Three-way quartz tube	Quartz
4	Flange (*a*)	Tapflon
5	Flange (*b*)	Tapflon
6	O-ring	Rubber
7	Cooling coil	Copper
8	Adapter for thermocouple (KF40)	Tapflon
9	Flange (*c*)	Tapflon

performance refrigerated circulator (JULABO, model Corio CD-200F). The maximum cooling temperature was 178 K.

In order to test its quality and heating performance, all of the main components were systematically connected and installed at beamline 5.2 SUT-NANOTEC-SLRI XAS at SLRI. Fig. 3 shows a photograph of the *in situ* XAS system showing its configuration.

The functionalities of the compact furnace were tested by recording the measured temperature inside the furnace under N_2 atmosphere at a flow rate of 10 ml min^{-1}. The heating temperature was ramped from room temperature to 1473 K with different heating rates of 2, 5, 10 and 20 K min^{-1}. Once the maximum temperature was reached, the furnace was held at 1473 K for at least 30 min to observe any thermal fluctuation. For all heating rates, the measured and set temperatures were well superposed, as shown in Fig. 4. Fig. 4 shows that the invented furnace achieved heating from room temperature to a maximum temperature of 1200 K with no thermal fluctuation during the tests at heating rates of 2, 5, 10 and 20 K min^{-1}.

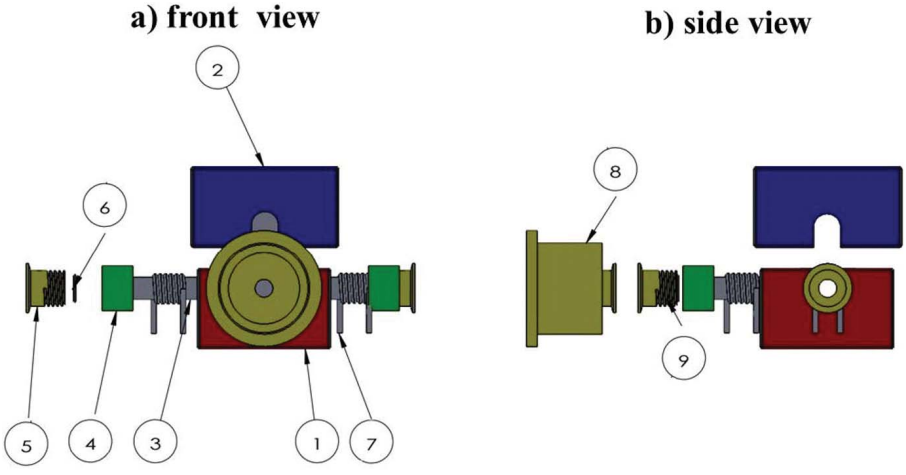

Figure 2
Main components of the *in situ* compact furnace: (*a*) top view and (*b*) side view. See Table 2 for description of numbers.

3. X-ray absorption spectroscopy

After furnace testing, *in situ* XAS experiments were carried out in order

Figure 3
In situ XAS system for transmission and fluorescence *in situ* XAS measurements.

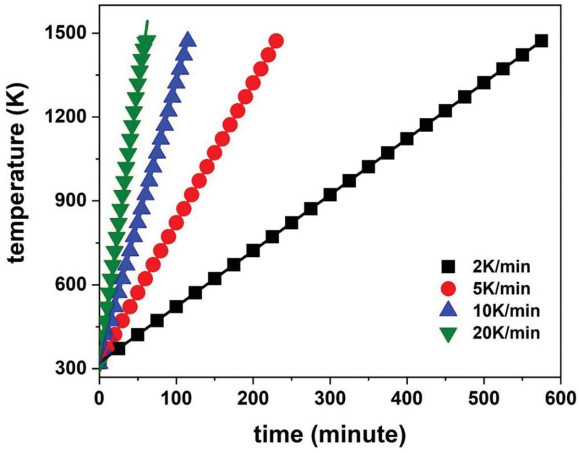

Figure 4
Set (symbol) and measured (line) temperatures as a function of time at heating rates of 2, 5, 10 and 20 K min^{-1}.

to study the reduction process of cationic ions in Pr_6O_{11} and NiO fine powders in transmission and fluorescence modes, respectively. In this section, we determine the effect of temperature on cationic oxidation state in Pr_6O_{11} and NiO compounds. Fine powders were ground and compressed into pellets of diameter 15 mm. Our furnace was set up and *in situ* XAS experiments were performed at beamline 5.2 to record the Pr and Ni XANES in transmission and fluorescence modes, respectively. The stored current was around 120 mA. Germanium (220) double single-crystals were utilized as a monochromator to probe the Pr and Ni elements at their L_3-edge (5964 eV) and *K*-edge (8333 eV), respectively. The data interval was set as 0.3 eV. The measurements were carried out at various temperatures ranging from 300 to 1473 K under H_2 reducing atmosphere. Using *Athena* software, the recorded XANES spectra were normalized and interpreted to study the changes in the oxidation states for Pr and Ni cations.

3.1. Pr L_3-edge XANES

Pr_6O_{11} commercial powder was compressed into a pellet of diameter 15 mm and placed at an angle of 90° in the sample holder. Heating steps were programed from room temperature to 1473 K with a heating rate of 10 K min^{-1}. Firstly, XAS measurements were made in transmission mode by probing Pr at its L_3 absorption edge at 5964 eV. The photon energy was tuned using the Ge (220) double-crystal monochromator. *In situ* XANES spectra were collected during heating the sample under H_2 atmosphere with a flow rate of 20 ml min^{-1}. Fig. 5 shows all the normalized spectra at various temperatures.

Consider a mixture of Pr^{3+} and Pr^{4+} cations in Pr_6O_{11} compound at ambient atmosphere. According to charge neutralization, the corresponding weight percentages are derived to be 33.3% and 66.7%, respectively. This resulted in an average oxidation state of +3.67. Based on the recorded XANES spectra, the corresponding absorption edge was located at a photon energy of 5968.1 eV. Main peaks at 5970.4 eV and 5981.2 eV contributed to $4f^2$ and $4f^1$ electronic configurations, respectively (Ogier *et al.*, 2019). As the temperature reaches 470 K, the absorption edge shifts significantly towards lower energy. This indicates the reduction of Pr ions: Pr^{4+} ions were partially reduced to Pr^{3+} ions. As a result, the intense peak of Pr^{4+} species at 5981.5 eV decreased as a function of temperature. This can be attributed to the increasing ratio of Pr^{3+}/Pr^{4+}. Furthermore, the white line peak of Pr^{4+} species at 5981.2 eV was absent when the reduction process was completely finished at 1273 K. This is in good accordance with the work of Luo *et al.* (2006), which reported that Pr_6O_{11} was reduced at high temperature and completely transformed to Pr_2O_3 around that temperature.

Moreover, we determined the weight percentage of the crystalline phases of Pr_6O_{11} and Pr_2O_3 during reduction under H_2 atmosphere by processing a linear combination fit (LCF) for the energy range −30 to 30 eV from the Pr L_3 absorption edge. The fit results are demonstrated in Table 3, and suggest

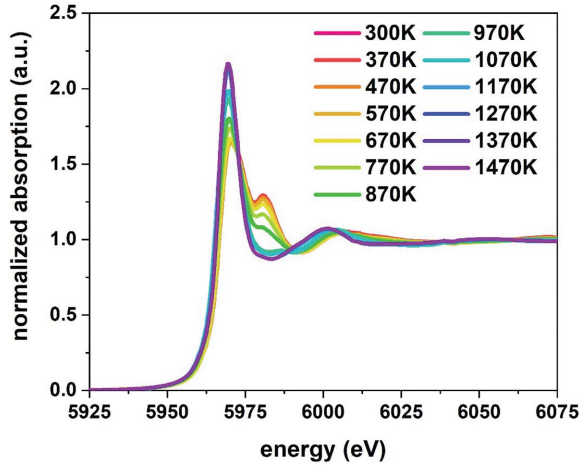

Figure 5
Normalized XANES spectra of Pr_6O_{11} measured at the Pr L_3-edge from 300 K to 1473 K.

Table 3
Weight percentages of Pr^{3+} and Pr^{4+} cations in the sample at various temperatures.

Temperature (K)	Pr^{3+} (wt%)	Pr^{4+} (wt%)	*R*-factor
300	33.3	66.7	0.001
370	36.8	63.2	0.003
470	40.6	59.4	0.005
570	45.7	54.3	0.005
670	51.9	48.1	0.005
770	54.5	45.5	0.006
870	69.7	30.3	0.008
970	85.5	14.5	0.011
1070	97.7	2.3	0.007
1170	99.7	0.3	0.000
1270	100.0	0	0.000
1370	100.0	0	0.000
1470	100.0	0	0.000

that *R*-factors of all fitting results are below 0.015, indicating high accuracy and reliability of the LCF fitting.

3.2. Ni *K*-edge XANES

NiO commercial powders were mixed with boron nitride powders in order to dilute the Ni content and compressed into pellets. A pellet was placed in the sample holder at an angle of 45° and loaded together into the center of the furnace for *in situ* fluorescence XAS operation. XANES measurements were carried out by probing Ni at 8333 eV. The *in situ* beamline configuration was set up as previously described in Section 3.1. Here, the SDD detector was utilized for measuring the XAS signal. The water cooling temperature was set at 283 K to prevent heat damage to the SDD. The heating steps were programmed from room temperature to 773 K to investigate the reduction process of Ni^{2+} ions in NiO compounds under H_2 flowing gas with a heating rate of 20 ml min^{-1}. Also, XANES spectra of Ni foil and NiO compound with space group *Fmc̄m* were recorded under ambient conditions and used as references for Ni^0 and Ni^{2+} species. The results are shown in Fig. 6.

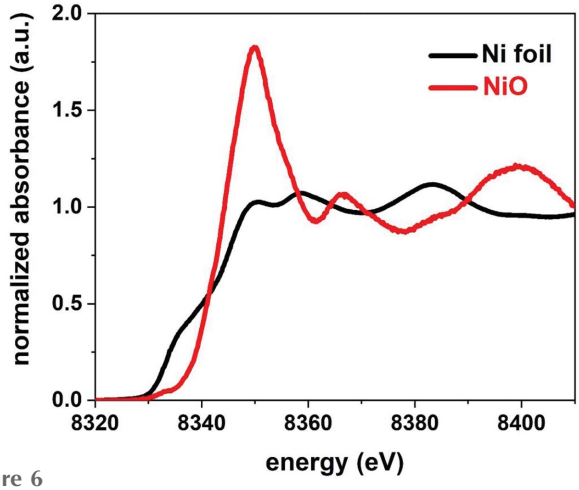

Figure 6
Ni *K*-edge XANES spectra of Ni foil and NiO compound, recorded at room temperature.

Table 4
Weight percentages of Ni^0 and Ni^{2+} species in NiO sample at various temperatures.

Temperature (K)	Ni^0 (wt%)	Ni^{2+} (wt%)	*R*-factor
370	1.7	98.3	0.0002
420	1.6	98.4	0.0002
470	0.9	99.1	0.0002
520	0.6	99.4	0.0002
570	0.5	98.5	0.0002
620	27.9	72.1	0.0002
670	75.6	24.4	0.0002
720	92.1	7.9	0.0002
770	100.0	0.0	0.0002

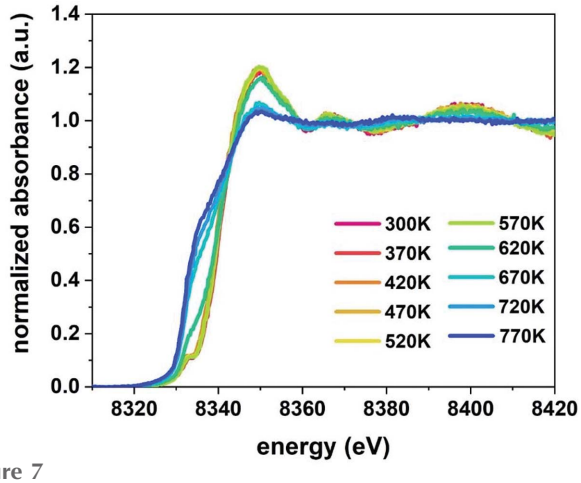

Figure 7
Ni *K*-edge XANES spectra of NiO compound recorded at various temperatures.

Fig. 6 shows absorption edges at 8333.3 eV and 8344.4 eV for Ni foil and NiO, respectively. As a result, these characteristic values can be used as references for Ni^0 and Ni^{2+} species.

Considering the Ni *K*-edge XANES spectra of NiO compound recorded at various temperatures (see Fig. 7), its absorption edge obviously decreased from 620 K. It is noteworthy that the intensity of the white line peak at 8351 eV, generated by scattering between central Ni atoms and surrounding O atoms, also declined. This suggests that Ni^{2+} ions were partially reduced to Ni^0 metallic species with increasing temperature. The spectrum recorded at 770 K is similar to that of the Ni foil. As shown in Table 4, the reduction process was completely finished at 770 K.

4. Conclusions

The design, fabrication and performance of a compact furnace for *in situ* heating XAS experiments have been described. The furnace can be easily installed at XAS synchrotron facilities for measurements in transmission and fluorescence modes from 300 to 1473 K with no heating fluctuation. The maximum heating rate exceeds 20 K min^{-1}. The experimental atmosphere can be controlled by flowing or mixing gas with an adjustable flow rate from 1 to 100 ml min^{-1}. The furnace was

successfully set up at beamline 5.2 (SLRI, Thailand) for *in situ* XAS operation. Transmission XANES spectra at various temperatures indicated the reduction of Pr ions in Pr_6O_{11} catalyst compounds under H_2 reducing atmosphere (average oxidation state from +3.67 to +3) and the phase transition $Pr_6O_{11} \rightarrow Pr_2O_3$ at 1173 K. Further, *in situ* XAS spectra of Ni in fluorescence mode showed the reduction of Ni^{2+} ions to Ni^0 metallic species at 620 K. Therefore, our furnace is very suitable for investigation of temperature-dependent structure transitions such as metallic melts, nanoparticles phase-change and the solidification process of crystalline materials.

Funding information

Funding and the well equipped machine shop were supported by the Synchrotron Light Research Institute (SLRI) in Thailand. This work has been partially supported by the Research Network NANOTEC (RNN) program of the National Nanotechnology Center (NANOTEC), National Science and Technology Development Agency (NSTDA), Ministry of Higher Education, Science, Research and Innovation (MHESI), Thailand.

References

An, P., Hong, C., Zhang, J., Xu, W. & Hu, T. (2014). *J. Synchrotron Rad.* **21**, 165–169.
Bokhoven, J. A. van, van der Eerden, A. M. J., Smith, A. D. & Koningsberger, D. C. (1999). *J. Synchrotron Rad.* **6**, 201–203.
Bolin, T. B., Wu, T., Schweitzer, N., Lobo-Lapidus, R., Kropf, A. J., Wang, H., Hu, Y., Miller, J. T. & Heald, S. M. (2013). *Catal. Today*, **205**, 141–147.
Boonruang, C., Thong-on, A. & Kidkhunthod, P. (2018). *Sci Rep*, **8**, 2289.
Chin, Y. Y., Lin, H., Hu, Z., Shimakawa, Y. & Chen, C. (2019). *Physica B*, **568**, 92–95.
Deb, A., Ralph, J. M., Cairns, E. J. & Bergmann, U. (2006). *Phys. Rev. B*, **73**, 115114.
Eerden, A. M. J. van der, van Bokhoven, J. A., Smith, A. D. & Koningsberger, D. C. (2000). *Rev. Sci. Instrum.* **71**, 3260–3266.
Grunwaldt, J.-D., Kappen, P., Hammershøi, B. S., Tröger, L. & Clausen, B. S. (2001). *J. Synchrotron Rad.* **8**, 572–574.
Hashimoto, T., Yoshiasa, A., Okube, M., Okudera, H. & Nakatsuka, A. (2007). *AIP Conf. Proc.* **882**, 428–430.
Huwe, H. & Fröba, M. (2004). *J. Synchrotron Rad.* **11**, 363–365.
Inukai, K., Iwai, H., Takahashi, Y. & Shin, W. (2015). *Ceram. Int.* **41**, 2852–2862.
Jaiban, P., Watcharapasorn, A., Yimnirun, R., Guo, R. & Bhalla, A. S. (2018). *J. Alloys Compd.* **759**, 120–127.
Kappen, P., Grunwaldt, J., Hammershøi, B. S., Tröger, L. & Clausen, B. S. (2001). *J. Catal.* **198**, 56–65.
Lamberti, C., Prestipino, C., Bordiga, S., Berlier, G., Spoto, G., Zecchina, A., Laloni, A., La Manna, F., D'Anca, F., Felici, R., D'Acapito, F. & Roy, P. (2003). *Nucl. Instrum. Methods Phys. Res. B*, **200**, 196–201.
Luo, M.., Yan, Z.. & Jin, L.. (2006). *J. Mol. Catal. A*, **260**, 157–162.
Marini, C., Diaz-Rovira, A. M., Kennedy, B. J. & Joseph, B. (2018). *J. Mater. Eng. Perform.* **27**, 6322–6327.
Massa, N. E., Ramos, A. Y., Tolentino, H. C. N., Sousa-Neto, N. M., Fonseca, J. Jr & Alonso, J. A. (2015). *Mater. Res. Expr.* **2**, 126301.
Mastelaro, V. & Zanotto, E. (2018). *Materials (Basel)*, **11**, 204.
Mathisen, K., Kirste, K. G., Hargreaves, J. S. J., Laassiri, S., McAulay, K., McFarlane, A. R. & Spencer, N. A. (2018). *Top. Catal.* **61**, 225–239.
Meneses, C. T., Flores, W. H., Sotero, A. P., Tamura, E., Garcia, F. & Sasaki, J. M. (2006). *J. Synchrotron Rad.* **13**, 468–470.
Ogier, T., Prestipino, C., Figueroa, S., Mauvy, F., Mougin, J., Grenier, J. C., Demourgues, A. & Bassat, J. M. (2019). *Chem. Phys. Lett.* **727**, 116–120.
Ravel, B. & Newville, M. (2005). *J. Synchrotron Rad.* **12**, 537–541.
Song, T., Yao, W., Kiadkhunthod, P., Zheng, Y., Wu, N., Zhou, X., Tunmee, S., Sattayaporn, S. & Tang, Y. (2020). *Angew. Chem. Int. Ed.* **59**, 740–745.
Sriplai, N., Koowattanasuchat, S., Kidkhunthod, P., Chanlek, N., Eichhorn, S. J. & Pinitsoontorn, S. (2018). *J. Alloys Compd.* **739**, 19–29.
Steiner, C., Gänzler, A. M., Zehentbauer, M., Hagen, G., Casapu, M., Müller, S., Grunwaldt, J. & Moos, R. (2019). *Top. Catal.* **62**, 227–236.
Sumrunronnasak, S., Chanlek, N. & Pimpha, N. (2018). *Mater. Chem. Phys.* **216**, 143–152.
Tamura, K., Inui, M. & Hosokawa, S. (1995). *Rev. Sci. Instrum.* **66**, 1382–1384.
Yamamoto, Y., Suzuki, A., Tsutsumi, N., Katagiri, M., Yamashita, S., Niwa, Y., Katayama, M. & Inada, Y. (2018). *J. Solid State Chem.* **258**, 264–270.
Yao, W., Armstrong, A. R., Zhou, X., Sougrati, M. T., Kidkhunthod, P., Tunmee, S., Sun, C., Sattayaporn, S., Lightfoot, P., Ji, B., Jiang, C., Wu, N., Tang, Y. & Cheng, H. M. (2019). *Nat. Commun.* **10**, 3483.
Zhao, N., Yao, M. J., Ma, H. T. & Wong, C. P. (2017). *J. Mater. Sci. Mater. Electron.* **28**, 8824–8831.